WILEY-VCH

RESEARCH ARTICLE

Acidity of Isomorphic Substituted Zeolites with B, Al and Ga Revisited

Andre Nicolai Petelski,*[a] Nélida María Peruchena[b] and María Fernanda Zalazar*[b]

[a] Dr. A. N. Petelski
Departamento de Ingeniería Química
Universidad Tecnológica Nacional (UTN), Facultad Regional Resistencia (FRRe), CONICET, Centro de Investigación en Química e Ingeniería Teórica y Experimental (QUITEX), French 802, H3500CHJ, Resistencia, Chaco, Argentina.
E-mail: npetelski@frre.utn.edu.ar

[b] Prof. Dr. N. M. Peruchena, Prof. Dr. M. F. Zalazar
Laboratorio de Estructura Molecular y Propiedades (LEMyP), Instituto de Química Básica y Aplicada del Nordeste Argentino (IQUIBA-NEA), Consejo Nacional de Investigaciones Científicas y Técnicas, Universidad Nacional del Nordeste (UNNE-CONICET),
Avenida Libertad 5460, 3400 Corrientes, Argentina.
E-mail: mfzalazar@conicet.gov.ar

Supporting information for this article is given via a link at the end of the document.

Abstract: Isomorphic substitution of zeolites with B, Al and Ga is a widely used approach in catalysis. The experimentally reported trend of their acidities decreases in the order: Al > Ga > B. However, a consistent explanation is still lacking in the literature. To bring more understanding of this trend, density functional theory computations were conducted on several model systems. First, the acidity of small clusters with two (2T) and five (5T) tetrahedral sites was analyzed. These systems were then projected onto three large void structures: H-[A]-BEA (52T), H-[A]-FAU (84T) and H-[A]-MOR (112T) with A = B, Al, Ga. Our electron density and Interacting Quantum Atom analyses show that the acidity of Al zeolites originates from the much stronger O–Al bond, which is dominated by the electrostatic attraction. The bridging hydroxyl therefore donates more charge density to the metal, the proton becomes more positive and consequently more acidic. Ga zeolites are more acidic than B zeolites due to the greater covalent nature on the O–Ga bond. The resulting acidity, as seen by ammonia, depends on both the acidic oxygen and the charge distribution of the surrounding oxygens exerted by the substituents.

Introduction

Isomorphically substituted zeolites occupy a prominent position as solid acid catalysts in the current industry. Within the boron family, the first three elements, boron (B), aluminum (Al), and gallium (Ga), have been extensively used to modulate the acidity of zeolites, and consequently their catalytic[1] and adsorptive activities.[2] Aluminum is distinguished for promoting more acidic zeolites than any other element. Despite there is a consensus about the trend in acidities (being Al(OH)Si > Ga(OH)Si > B(OH)Si) and a plethora of experimental observations,[3] there is still no fundamental understanding on this topic. The first attempt to explain the acid strength was the electronegativity scale of Sanderson,[4] which is simply based on the chemical composition of the zeolites. Since Ga did not follow the rule, new electronegativity values were then proposed.[5] Later, using molecular electrostatic potential maps on 8T models, Chatterjee et al.[6] showed that Al causes a more polarized environment than B. Then, the authors explain the trend in terms of polarizability. Li et al.[7] explained the trend for the set Al, Ga and Fe using Bader's atomic charges . However, these authors were unable to answer what the underlying mechanism is, whether the phenomenon is due to purely electrostatic effects, or whether there is some degree of covalency. In particular, the authors are not able to explain why zeolites with Al are slightly more acidic than those with Ga.

Regarding the intrinsic acidity of zeolites, there have been several efforts to predict the acid strength of different topologies. The most common descriptor is the deprotonation energy (DPE).[8] Though it is still computed, some authors have criticized its usefulness. For instance, the DPE is influenced by the size and type of the cavity.[9] Besides, the incompleteness of the DPE arises from its incapacity to be decomposed into its covalent and ionic components.[10] Other acidity descriptors found in the literature include O–H bond lengths and frequencies,[11] bond orders,[12] atomic charges of the proton,[13] and the critical point derived from the Laplacian of the electron charge density.[14]

On the other hand, the acidity of a particular topology is experimentally measured via adsorption of several molecular probes. Among others, one of the most used is ammonia.[15] This method includes measurement of the desorption temperature and the determination of adsorption enthalpies associated with the proton transfer process.[3a,16] Nevertheless, it has been argued that ammonia cannot really sense the intrinsic acidity of the relevant sites because the adsorption process is masked by the dispersion forces related to confinement effects[17,18] Yet, these

interactions, which are unrelated to acid strength, have not been formally identified.

The aim of this work is to understand the physical reason behind the acid trend and what the implications are in the real cavity. To this end, B, Al, and Ga were chosen as substituent elements. For our investigations, we performed density functional theory (DFT) computations at the M06-2X level of theory over different model clusters and progressively increasing their sizes. We found out that the acid strength of Al-substituted topologies is produced by a stronger electrostatic attraction between Al and the bridging OH. In contrast, the fact that Ga promotes a more acidic proton than B is due to the stronger covalent nature of the O-Ga bond. The elements also build up different charge distributions within the cavities, which affects the final acidity as measured by ammonia. Pnictogen bonds between N and O atoms are also decisive for the stabilization of the adsorbate.

Computational Methods

All computations were performed with Gaussian 16.[19] Molecular clusters with two and five tetrahedral sites, 2T and 5T (T = Si, A and A = B, Al, Ga as tetrahedral atoms) respectively, were optimized with the M06-2X hybrid functional of Truhlar and Zhao[20] along with the 6-311++G(2d,2p) basis set. This functional has a demonstrated capacity to reproduce experimental values within several zeolite systems.[21] The 5T and extended models were built by taking three zeolite topologies from the International Zeolite Association online database:[22] BEA (Beta), FAU (Faujasite) and MOR (Mordenite). We then considered 5 tetrahedral Si atoms (one bonded to the acidic oxygen and three near the A atom) and replaced the O atoms by H at the same direction of the terminal O atoms.

To consider the whole topology of the cavity, the selected zeolite structures have been modeled by an extended 52T quantum cluster model for H-[A]-BEA, 84T for H-[A]-FAU and a 112T for H-[A]-MOR. The active site was positioned at the intersection channel for BEA, at the T1 site for FAU and at T4 site for MOR (at the intersection between the 12-ring (12R) channel and the 8R side-pockets). For all models, the terminal silicon atoms were saturated with hydrogen atoms at a bond distance of 1.47 Å along the Si-O bond. These fictitious H atoms were kept fixed during the optimization to guarantee the environment of the corresponding zeolite. Similar cluster models were used in our previous work.[23] For these larger clusters, the calculations were performed using the two-layer ONIOM methodology,[24] at the M06-2X/6-31+G(d):PM6 level and the Gaussian 16 software.[19] The ONIOM model was defined as 16T/52T for BEA, 18T/84T for FAU and 16T/112T for MOR zeolites, with 16T and 18T being the high layer, while the remaining atoms of the model are the lower layer (see Figure S1 in the Supporting Information for further details). Adsorbates within the cavity were treated as part of the high layer. Electron densities and energies were obtained at M06-2X/6-31++G(d,p) level of theory.

To study the host-guest interactions between ammonia and the larger cluster models, both adsorption and protonation modes were tested during geometry optimizations. Only the most stable structures were selected. For all the *n*T (*n* = 2, 5, 52, 84, 112) cluster model, the adsorption energy (ΔE_{ads}) of ammonia was calculated by [Equation (1)]:

$$\Delta E_{ads} = E_{nT^*} - \left(E_{nT} + E_{NH_3}\right) \quad (1)$$

where E_{nT^*} is the total energy of the optimized adsorbed complex, E_{nT} the total energy of the isolated cluster and E_{NH_3} the total energy of the isolated ammonia.

Molecular electrostatic potentials (MEP) were mapped on the electron densities with an isosurface of $\rho(r) = 0.001$ a.u., and the corresponding $V_{S,max}$ values were computed with the Multiwfn software[25] and represented with VMD.[26] Voronoi deformation density (VDD) charges[27] Q^{VDD} (N) on the model clusters were also computed with the Multiwfn software.[25] These charges indicate the number of electrons that flows into ($Q^{VDD} < 0$) or out of ($Q^{VDD} > 0$) the Voronoi cell (N) as the result of the interaction between the two molecular fragments. All wave functions for 2T and 5T models were obtained at the M062X/6-311++G(2d,2p) level using Gaussian 16.[19]

All figures were created with CYLview[28] and VMD.[26]

Results and Discussion

2T Clusters

We started by analyzing the disiloxane model ($H_3Si{-}O{-}SiH_3$). When a Si atom is substituted by either B, Al or Ga a disproportion of charges is created so that the O atom acquires a negative charge: $H_3Si{-}(O^-){-}AH_3$. This negative charge can be counterbalanced by a proton $H_3Si{-}(OH){-}AH_3$ or other cations such as Na^+. In the first case, the central oxygen has acidic properties. The bond between O and the substituent atom A is sometimes represented by dots $H_3Si{-}(OH)\cdots AH_3$. However, the nature of this bond depends on several factors (*vide infra*).

Figure 1 shows three conformers of the $H_3Si{-}(OH){-}AH_3$ molecule along with two parameters that could evaluate the acidity of the proton. The $V_{S,max}$ is the maximum value of the electrostatic potential map function, while the VDD charges reflect how much charge is going out (Q > 0) or into (Q < 0) the Voronoi cell of the atom, in this case the proton. Therefore, the more positive these values are, the more acidic the H. As can be seen in Figure 1, all conformers with Al show the most positive values for both parameters, followed by B and Ga. These simple models cannot reproduce the trends observed in zeolites; however, they still capture the acidic strength of hydrogen within the system with Al. Among the large variety of molecules used to measure the acidity of Brønsted acid sites (BAS) in zeolites, ammonia is one of the most commonly used.[15] We used this molecule as a probe to test the acidity of the 2T*b* models, because they have larger $V_{S,max}$ and VDD charge values. Figure 2 displays the interaction energies between NH_3 and $H_3Si{-}OH{-}AH_3$ upon hydrogen bonding with the acid site. Again, the 2T*b* cluster with Al shows the strongest interaction energy with ammonia. In line with this result, the system with Al displays the shortest *d*(H···N) hydrogen bonding distance, and the largest O–H stretching. Another interesting feature is the bond distance between O−A atoms that follows the order of atomic radii: O−B < O−Al < O−Ga. To find out why the 2T

cluster with Al has the most acidic proton we evaluated the nature of the bond between O and B, Al and Ga.

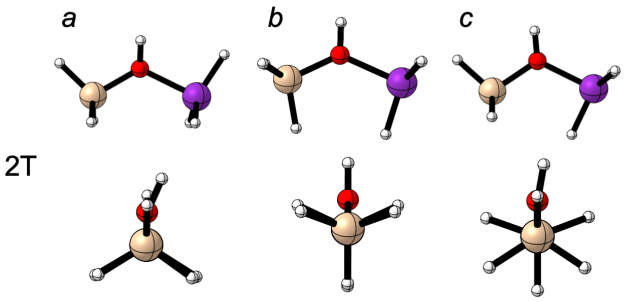

A	$V_{S,max}$	VDD	$V_{S,max}$	VDD	$V_{S,max}$	VDD
B	71.6	277	72.0	281	72.6	277
Al	75.6	286	76.2	295	76.4	286
Ga	69.6	258	70.0	261	69.4	257

Figure 1. Figure Top: front and side views of $H_3Si{-}OH{-}AlH_3$ structures. Bottom: Values (in kcal mol^{-1}) of Maximum electrostatic potentials ($V_{S,max}$) and Voronoi Deformation Density (VDD) charges (in me$^-$) on the acidic protons of $H_3Si{-}OH{-}AH_3$ structures.

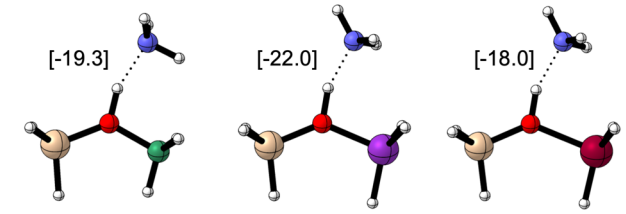

	B	Al	Ga
d(H···N)	1.60	1.58	1.65
Δd(O−H)	0.06	0.07	0.05
d(O−A)	1.70	2.01	2.21

Figure 2. Corrected interaction energies (in kcal mol^{-1}) between acidic protons (−OH) and ammonia computed at M06-2X/6-311++G(2d,2p). Geometrical distances are also displayed in Å. The O−H bond length of the isolated cluster is 0.96 Å for all systems.

First, we separated the $H_3Si{-}OH{-}AH_3$ cluster (2T*b*) into two fragments that are also neutral molecules: the H_3Si-OH silanol moiety and the borane BH_3, alane AlH_3 and gallane GaH_3 hydrides, such that the interaction is $H_3Si{-}O(H)\cdots AH_3$. We then computed the bonding energies ΔE_{bond} [Eq. (2)] as the difference between the energy of the optimized silanol moiety (SiOH) and the energy of the optimized hydrides (AH_3), and the results are collected in Table 1.

$$\Delta E_{bond} = E(SiOH\text{-}AH_3) - E_i(SiOH) - E_i(AH_3) \quad (2)$$

Here, E_i stands for *energy of the isolated fragment*. The energy needed to deform the monomers from their isolated states to the structures they acquire in the 2T clusters was computed by [Equation (3)], and the actual energy between the deformed structures, this is the O···A interaction energy, was computed by [Equation (4)]:

$$\Delta E_{strain} = [E(SiOH) - E_i(SiOH)] + [E(AH_3) - E_i(AH_3)] \quad (3)$$

$$\Delta E_{int\text{-}O\cdots A} = E(SiOH\text{-}AH_3) - E(SiOH) - E(AH_3) \quad (4)$$

Therefore, the bonding energy is expressed as $\Delta E_{bond} = \Delta E_{strain} + \Delta E_{int\text{-}O\cdots A}$.

Table 1. Bonding analysis (in kcal mol^{-1}) between silanol and AH_3 hydrides (A = B, Al and Ga).

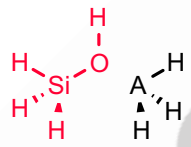

Fragment 1	Fragment 2	ΔE_{bond}	ΔE_{strain}	$\Delta E_{int\text{-}O\cdots A}$
H_3SiOH	BH_3	−13.4	9.4	−22.8
	AlH_3	−20.8	3.8	−24.7
	GaH_3	−15.0	1.6	−16.5

As shown in Table 1, the O−Al bond has the strongest bonding energy (-20.8 kcal mol^{-1}) and interaction energy (-24.7 kcal mol^{-1}). The large deformation energy of borane[29] is responsible for the lowest ΔE_{bond} within the $H_3Si{-}OH\cdots BH_3$ complex. When looking at the absolute value of interaction energies between O and A atoms, the trend matches with the acidic strength of the 2T clusters: $|\Delta E_{int\text{-}O\cdots Al} > \Delta E_{int\text{-}O\cdots B} > \Delta E_{int\text{-}O\cdots Ga}|$.

Finally, we then analyzed two other aspects of the O···A bonds: their electrostatic attraction and covalent features. Figure 3a displays the MEP maps along with their surface extrema ($V_{S,max}$ and $V_{S,min}$). The AlH_3 fragment shows the most positive value on the ESP surface (87.3 kcal mol^{-1}) against 64.5 and 69.5 kcal mol^{-1} within BH_3 and GaH_3 respectively. Hence, following the concept of the sigma hole, one would expect a stronger electrostatic attraction between the silanol and the alane. To further analyze this idea, we computed the electrostatic and covalent contributions to the interaction energy between the silanol and the AH_3 moieties within the framework of the Interacting Quantum Atoms at constrained geometries (IQA, see Table S1 in the Supporting Information file). We fixed the O···A distances at 2 Å to exclude the influence of the different distances and to reveal the pure effect on the acidic proton. This "consistent geometry" approach has demonstrated more clarity and more insights when analyzing energetic components that are distance dependent.[30] Our results demonstrate that the classical contribution E_{cl} between the fragments is the largest for the system with Al: -48.3 kcal mol^{-1} against −15.7 and −26.4 kcal mol^{-1} within $H_3SiOH\cdots BH_3$ and $H_3SiOH\cdots GaH_3$ respectively. Even more, when analyzing the interatomic interactions, the O−Al bond also shows the largest classical interatomic contribution E_{cl} (see Table S2). Besides, the values of Table S2 for O−A bonds show features of ionic bonds:[31] a small and stabilizing contribution of E_{xc}, while the coulombic part is dominant. e.g., in $H_3Si{-}OH{-}AlH_3$, E_{xc}(O, Al),

and E_{cl}(O, Al) are −23.1 and −544.8 kcal mol^{-1}, respectively. Therefore, we can confirm that the larger accumulation of positive charge around the aluminum atom and negative charge around the oxygen atom of the hydroxyl group are responsible for the more stabilizing electrostatic interaction.

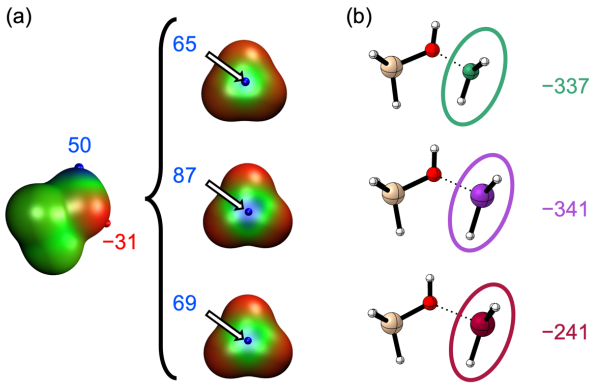

Figure 3. (a) Values of Maximum electrostatic potentials ($V_{S,max}$) on H_3Si-OH and AH_3 (A = B, Al, Ga) fragments. (b) Voronoi Deformation Density (VDD) charges (in milli electrons) on the AH_3 fragments.

Figure 3 also displays the VDD charges (in me$^-$) over the Voronoi cells of AH_3 fragments. They represent how much charge goes into the AH_3 Voronoi cells and, therefore, how much charge flows out of the silanol moiety. The BH_3, AlH_3 and GaH_3 fragments experience a gain of –337, –341 and –241 me$^-$ respectively. These values indicate that the silanol fragment donates more charge within the system with Al. These observations are similar to those of Nieuwland and Fonseca Guerra [32] for carboxamides, thioamides, and selenoamides. They found out that the amine group has a stronger hydrogen bond donor ability within the systems with Se because the N lone pair donates more charge to the $\pi^*_{C=Se}$ orbital than in the other systems.

Finally, one of the most used parameters to measure the intrinsic acid strength is the DPE.[8] It has been claimed that one of the reasons of its incompleteness is the lack of information about the ionic and covalent components.[10] The IQA scheme can give an approximation to these components but on the OH bond itself. **Table S2** in the Supporting Information shows the IQA coulombic and covalent components of the acidic O−H bond. These values are typical of polar covalent bonds, with the O−H bond having the largest coulombic component within the systems with Al.

5T Clusters

In this section, we analyze the nature of the acidic proton H and O−A bonds in structures with five tetrahedral sites taken from three zeolites: BEA, FAU and MOR. Here we define the acidic oxygen as Oa and the other three O atoms bonded to the A atom as Ob, this is: SiH_3−Oa(H)−A(Ob−SiH_3)$_3$. The molecular structures are shown in Figure 4 along with VDD charges over the acid proton and AOb_3 fragments within the 5T structure. The Al-5T clusters hold the most positive protons. This is, larger $V_{S,max}$ and VDD values. The trend in acidity now matches the experimental trend: Al > Ga > B.

The (AOb_3) regions denoted by the dashed lines of Figure 4 indicate how much charge goes into the AOb_3 Voronoi cells. These values are in agreement with our previous observation for 2T clusters. Al-5T clusters are more acidic than those with B and Ga because more charge is flowing out from the silanol moiety to the $AlOb_3$ Voronoi cell. This charge transfer also takes charge density away from the H atom, thus, making it more positive. The two maxima values of the MEP and VDD charges give an idea of the acidity, but they are not mutually correlated. For instance, in all Al-5T clusters the $V_{S,max}$ values are almost 76 kcal mol^{-1}, but the VDD charges are 313, 310 and 330 milli-ellectrons for 5T-BEA, FAU and MOR respectively.

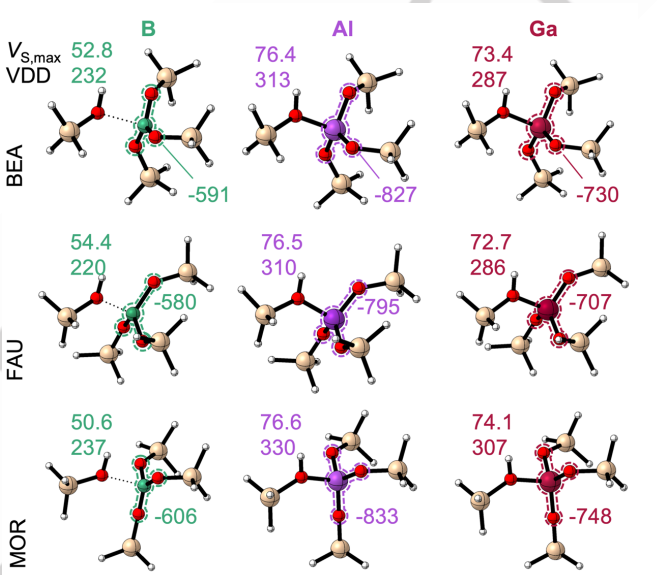

Figure 4. Values of Maximum electrostatic potentials $V_{S,max}$ (kcal mol^{-1}) and Voronoi Deformation Density (VDD) charges (milli-electrons) on the acidic protons of 5T model structures of BEA, FAU and MOR zeolites. Dashed lines indicate the VDD charges over the voronoi cell containing A(Ob)$_3$ fragments.

Here we can also separate the 5T clusters into neutral fragments: the SiH_3−OaH silanol moiety and A(Ob−SiH_3)$_3$ fragments. The interaction between these fragments, as shown in Table 2, is again higher for the Al-5T clusters. The $V_{S,max}$ values of the A(Ob−SiH_3)$_3$ fragments follow the same order than those obtained for the smaller 2T systems (see Figure S2). For instance, within 5T-BEA systems, the $V_{S,max}$ are 39, 132 and 101 kcal mol^{-1} for B, Al and Ga respectively. When analyzing the electrostatic nature of the interatomic O−A interactions, we found out again that the O−Al bond has the largest electrostatic component for each 5T model (see Tables S3 in the Supporting Information). The E_{elec} (IQA) values range from –634 to –645 kcal mol^{-1} for Al-5T clusters, while the same component ranges from –456 to –496 kcal mol^{-1} for B- and Ga-5T clusters. To avoid the effects of different interatomic O−A distances, all the A-BEA models were constrained at the same O−A distance (1.8665 Å). As shown in Table S4, even at the same interatomic distance, the model system with aluminum has an O−A bond with a larger electrostatic

component and a stronger interatomic interaction. Overall, the IQA method clearly demonstrates that the silanol moiety donates more charge density to Al because of a more attractive electrostatic interaction.

Table 2. Interaction energies ($\Delta E_{int\text{-}O\cdots A}$) and adsorption energy (ΔE_{ads}) for adsorbed ammonia on 5T clusters (kcal mol^{-1}) computed at M06-2X/6-311++G(2d,2p) level of theory.

5T cluster[b]	$\Delta E_{int\text{-}O\cdots A}$	ΔE_{ads}
B-BEA	–4.7	–13.9
Al-BEA	–39.4	–22.1
Ga-BEA	–30.9	–21.6
B-FAU	–3.6	–12.6
Al-FAU	–36.7	–21.3
Ga-FAU	–28.0	–20.7
B-MOR	–1.9	–12.4
Al-MOR	–35.7	–26.2
Ga-MOR	–26.7	–26.7

The adsorption of the probe molecule is also consistent with the acidity trends. However, protonation is only observed within the Al- and Ga-MOR models as shown by the interaction energies of Table 2 (optimized structures of the adsorbed complexes are shown in Figure S3).

BEA, FAU and MOR zeolites

Now that we know how aluminum promotes more acidic protons, in this section we will analyze the behavior of the VDD charges within the cavity of the largest zeolite clusters. Within the large void structures of BEA, FAU and MOR, the intrinsic acidity matches the experimental trend: Al > Ga > B. As shown in Figure 6**,** the VDD charge over the acidic proton is the largest for every zeolite with aluminum. In line with previous results for the 5T clusters, the [$AlOb_3$] fragments experience the largest charge density income to the Voronoi cell. For example, VDD [AOb_3] = –570, –707 and –321 me$^-$ for B-, Al- and Ga-BEA respectively. Our values also suggest that BEA is the most acidic structure, followed by either FAU or MOR. While the trend in acidity is consistent with the observed acid strength for elements B, Al, and Ga, it is important to note that the trend based on different topologies deviates from the experimental results. This is simply because, although the model can capture the nature of the acidity, the VDD charge only measures one site. Besides, there are several other contributing factors that are outside of this model, such as acidity heterogeneity within the same zeolite structure, the different location of BAS inside pores, cavities, and channels (resulting in different environments), the Si/A ratio, among others. At this point we are unable to compute the IQA electrostatic and covalent components of the O−A bonds because of the size of the systems. Nevertheless, the VDD charges follow the same trends as those observed within the 5T systems.

Ammonia adsorption on BEA, FAU and MOR zeolites

O−H bond distances (Table 3, see also Table S5) show that ammonia is protonated in all zeolites substituted with both Al and Ga. For the adsorption in B-substituted zeolites, the results show that ammonia become protonated on the acid site only for B-BEA zeolite and the B atom acquires a tetrahedral coordination. For B-FAU zeolite, the most stable structure involves the adsorbed ammonia complex, and no protonation is observed (the O−H bond distance is shorter: 1.08 Å). The B···Oa distance is intermediate between tetrahedral and trigonal coordination. For the B-MOR zeolite, both structures are found, the most stable corresponding to the adsorbed complex where no proton transfer is observed, and the B atom remains trigonal (see Table 3). For the A-BEA zeolites, the O−H bond distances are around 1.5 Å, and the ΔE_{ads} energies are also around −30 kcal/mol. According to the expected acidity of the cluster models, the stability order of the adsorbed complexes is the following BEA > FAU > MOR. This order is also consistent with the estimated acidities with the VDD charges over the acidic proton.

By using extended cluster models, not only the interaction with acidic and basic sites is considered, but also the confinement effects of the solid on the adsorbed molecule. The adsorption of NH_3, as well as other molecules, is strongly influenced by interactions such as hydrogen bonding and dispersion forces. It has been stated that these interactions are not necessarily indicative of acid strength and are often unrelated to it.[17,18] In the smaller BEA zeolite, although the probe molecule is small relative to the cavity, protonation is favored (protonation occurs with the proton of the BAS, but N–H···O type interactions with the zeolite walls are also favored). These interactions can be visually revealed with the reduced density gradient approach,[36] as shown in Figure 6 (the contour plots of all systems are shown Figure S4, see also the Supporting Discussion 1). All the topologies exhibit a highly directional hydrogen bond that can be seen as a blue disk (inset 1 in Figure 6). This hydrogen bond is supported by other interactions such as a second and weaker hydrogen bond (inset 2 in Figure 6),[37] and a pnictogen bond between O and N atoms (inset 3 in Figure 6). In terms of the sigma hole concept, this pnictogen bond can be understood as an electrostatic interaction between the positive region of N (see maxima values of its electrostatic surface in Figure S6) and the negative region of O associated to its lone pair. It should be mentioned that this type of interaction also accounts an important orbital contribution.[38] These other host-guest interactions are related to the confinement effects of the zeolite framework (these host-guest interactions are not present in the smaller cluster models, only when the catalyst cavity is considered.).[39]

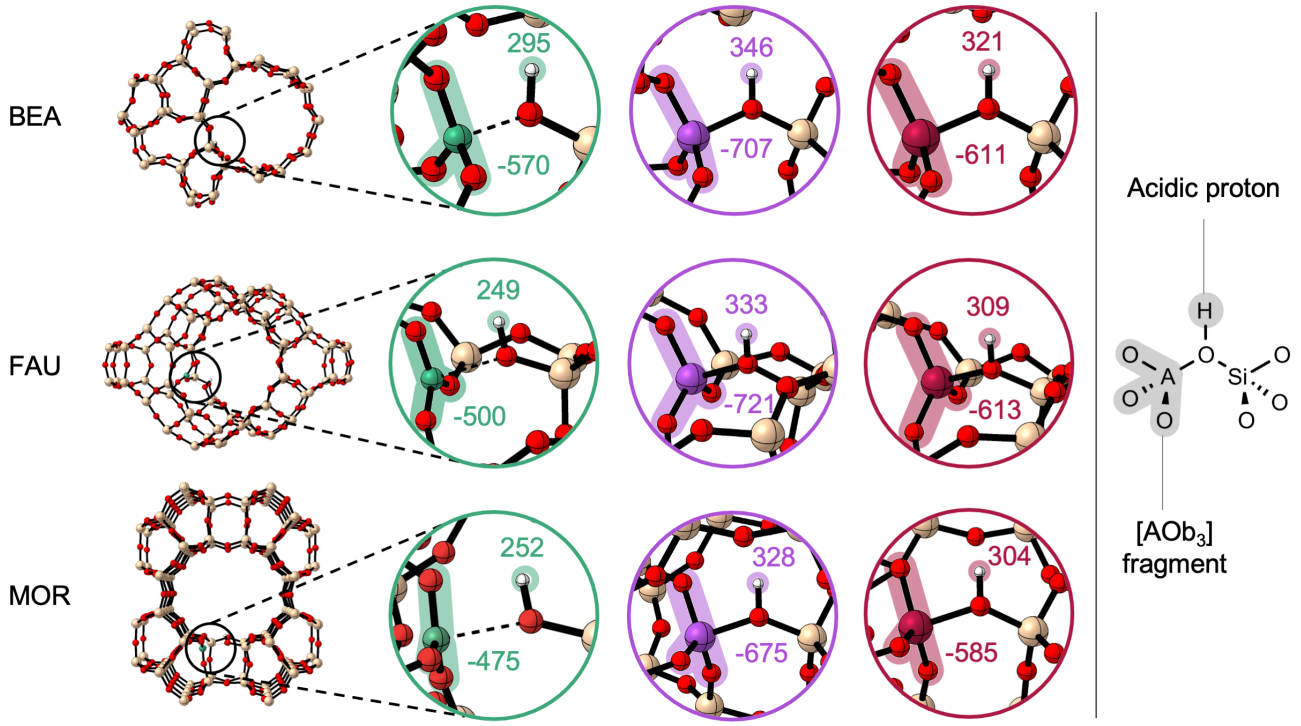

Figure 5. Voronoi deformation density charges (milli-electrons) over the highlighted voronoi cells of the acidic proton [H] and [AOb_3] fragments. Wave functions computed at M06-2X/6-31++G(d,p).

Table 3. Adsorption energies (kcal mol^{-1}) and selected bond distances (Å) for adsorption of ammonia on BEA, FAU and MOR zeolites computed at ONIOM-M06-2X/6-31+G(d):PM6 level.

Zeolites	ΔE_{ads}[a]	d(A···Oa)	d(A···Ob)[b]	d(O−H)
B-BEA	−26.2	1.53	1.47	1.50
Al-BEA	−33.4	1.76	1.73	1.56
Ga-BEA	−32.1	1.83	1.81	1.50
B-FAU	−15.1	1.71	1.46	1.08
Al-FAU	−26.1	1.80	1.74	1.42
Ga-FAU	−27.7	1.86	1.81	1.43
B-MOR	−11.4	2.22	1.39	1.01
Al-MOR	−22.6	1.77	1.72	1.50
Ga-MOR	−25.8	1.86	1.81	1.47

[a] The experimental heat of ammonia adsorption is in the range of 28.7-35.8 kcal mol^{-1} for Al-BEA,[33] 28.7-31 kcal mol^{-1} for Al-FAU (Si/Al=2.4)[34] 38.2 kcal mol^{-1} for Al-MOR.[35] [b] The average bond length of the A atom to the three adjacent O atom, excluding Oa atom.

For BEA zeolites, the adsorption energies follow the sequence Al > Ga > B, in agreement with previous results. The lower adsorption energies found for B-containing zeolite complexes are consistent with their weak acid strength, which in turn explains their low catalytic activity. Recently, the esterification reaction of levulinic acid with different alcohols was tested using BEA zeolites containing hetero ions including Al, Ga and B.[40] The results showed that Al-Beta showed higher conversions compared to Ga-Beta (except with propanol), while B-Beta showed poor catalytic activity, which was attributed to its weak acid strength.

The ammonia complexes on Ga zeolites are more stable by 1.6 kcal mol^{-1} for FAU, and by 3.1 kcal mol^{-1} for MOR, when compared to the complexes adsorbed on Al zeolites. Thus, for FAU and MOR, stability decreases in the order Ga > Al > B and the stabilization does not follow the expected trend. This order of stability can be understood in terms of the interactions with specific regions of the acid site and with the zeolite framework. When analyzing the interaction pattern within the Al- and Ga-FAU structures (see also Figure S4), the ammonium cation forms a stronger ionic N^+–H···O^- hydrogen bond inside the Ga-FAU zeolite. This can be explained by the VDD charges associated to the surrounding O atoms. As shown in Figure S7, the O atom adjacent to Ga has a more negative charge than that in its Al counterpart, this is –406 me^- for Al-FAU and –428 me^- for Ga-FAU. The RDG contours of Figure S4 also show a stronger N^+–H···O^- within the Ga-FAU structure. The blue disk is barely visible, indicating is a very strong hydrogen bond.[36] Similar observations can be easily understood when analyzing the adsorption energies of Al- and Ga-MOR. The ammonium cation not only forms a stronger ionic N^+–H···O^- hydrogen bond with the gallium acid site, but also a stronger N^+···O^- pnictogen bond. In this case, the more negative O atom bonded to Ga forms a stronger N^+···O^- pnictogen bond (see Figure S7)

Although 5T clusters show the same trend in acidity, no such protonation was observed except for Al- and Ga-MOR. The reason can be clearly seen when considering the entire topology of the cavity. Confinement effects play a fundamental role in stabilizing the adsorbate, as the ammonium cation can form more interactions with the environment. The final "observed acidity" by the probe molecules will then depend on the average contribution of all the interactions with the acid site. Our computations suggest that the surrounding O atoms can also define this acidity, as Al and Ga promote different charge distributions on the same acid site, and on different cavities.

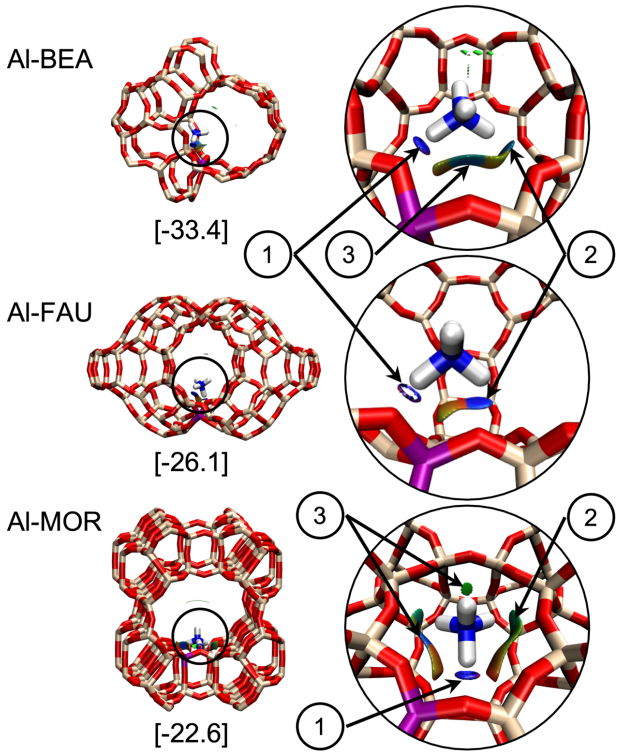

Figure 6. Contour plots of the reduced density gradient isosurfaces (density cutoff = 0.3 au) for all the zeolites with Al computed with a promolecular density. The blue and green surfaces indicate attractive non-covalent interactions, and red surfaces indicate repulsive interactions. Insets: (1) Strong N–H···O, (2) weak N–H···O and (3) N···O. (See zoomed-in views of the surfaces in Figure S8 in the supporting information file)

Conclusion

Our quantum computational experiments based on electron density analyses revealed why aluminum-substituted zeolites are intrinsically more acidic than those with boron and gallium. The more acidic nature of Al-substituted zeolites results from an enhanced interaction between the metal and the bridging hydroxyl, which is dominated by electrostatic interaction. The greater accumulation of positive charge on Al causes a greater electrostatic attraction, which favors a greater flow of electron density from the bridging hydroxyl to the metal, resulting in an increase of positive charge on the acidic proton.

On the contrary, since B and Ga cause almost the same electrostatic polarization, Ga-substituted zeolites are more acidic than those with B because of a larger covalent character of the O–Ga bond. Thus, the acidity of Al-substituted zeolites is dominated by electrostatic interactions, while that of Ga-substituted zeolites is dominated by covalent interactions. The stronger the O–A bond the higher the acidity.

Small clusters with 2 and 5 tetrahedral sites can capture this phenomenon. However, they are unable to explain the acid nature as seen by a probe molecule. When considering a larger void structure, the acidity measured by ammonia adsorption will ultimately depend on the specific interactions between the adsorbate and the surface. The oxygen atoms bonded to either B, Al or Ga display different atomic charges that also depend on the topology of the zeolite. Thus, those oxygen atoms more negatively charged will form stronger ionic hydrogen bonds with the adsorbate. Even more, the $N^{+}\cdots O^{-}$ pnictogen bond plays a key role in stabilizing the protonated ammonia and contributes to the acidity as seen by the probe molecule.

VDD atomic charges and the reduce density gradient were reliable tools to analyze both the acid strength and the adsorptive activity in large voids structures. Our findings thus prove that intrinsic and observed acidity cannot be treated separately. This work then raises the need to analyze three interrelated aspects when considering the catalytic activity of zeolites: the topology, the active site, and the silicon substituent.

Supporting Information

The authors have cited additional references within the Supporting Information.[41]

Acknowledgements

National Scientific and Technical Research Council - Argentina (CONICET), National Agency for the Promotion of Research, Technological Development and Innovation (AGENCIA), Secretaría General de Ciencia y Técnica of the Universidad Nacional del Nordeste (SGCyT-UNNE) of Argentine, and Secretaría de Ciencia y Técnología (SCyT) of the Universidad Tecnológica Nacional – Facultad Regional Resistencia (UTN – FRRe) of Argentine.

Keywords: Acidity • Confinement • Electrostatic Interactions • Zeolites

[1] (a) G. Kumar, D. Liu, D. Xu, L. Ren, M. Tsapatsis, P. J. Dauenhauer, *Green Chem.* **2020**, *22*, 4147–4160. (b) P. Gao, Q. Wang, J. Xu, G. Qi, C. Wang, X. Zhou, X. Zhao, N. Feng, X. Liu, F. Deng, *ACS Catal.* **2018**, *8*, 69–74. (c) L. Ni, R. Khare, R. Bermejo-Deval, R. Zhao, L. Tao, Y. Liu, J. A. Lercher, *J. Am. Chem. Soc.* **2022**, *144*, 12347–12356

[2] V. A. Tuan, J. L. Falconer, R. D. Noble, *Microporus Mesoporus. Mater.* **2000**, *41*, 269–280.

[3] (a) C. T. W. Chu, C. D. Chang, *J. Phys. Chem.* **1985**, *89*, 1569–1571. (b) A. Palčić, V. Valtchev, *Appl. Catal., A* **2020**, *606*, 117795. [c] Q. Zhang, S. Gao, J. Yu, *Chem. Rev.* **2023**, *123*, 6039–6106.

[4] W. J. Mortier, *J. Catal.* **1978**, *55*, 138–145.

[5] D. H. Dompas, W. J. Mortier, C. H. Kenter, M. J. G. Janssen, J. P. Verduijn, *J. Catal.* **1991**, *129*, 19–24.

[6] A. Chatterjee, T. Iwasaki, T. Ebina and A. Miyamoto, *Microporous Mesoporous Mater.* **1998**, *21*, 421–428.

[7] S. Liu, Y. He, H. Zhang, Z. Chen, E. Lv, J. Ren, Y. Yun, X. Wen, Y.-W. Li, *Catal. Sci. Technol.* 2019, *9*, 2812–2827.

[8] M. Boronat, A. Corma, *Catal. Lett.* **2015**, *145*, 162–172.

[9] A. J. Jones, R. T. Carr, S. I. Zones, E. Iglesia, *J. Catal.* **2014**, *312*, 58–68.

[10] Mi. Trachta, O. Bludský, J. Vaculík, R. Bulánek, M. Rubeš, *Sci. Rep.* **2023**, *13*, 12380.

[11] (a) A. Zecchina, G. Spotoab, S. Bordiga, *Phys. Chem. Chem. Phys.* **2005**, *7*, 1627–1642. (b) Y. Wang, D. Zhou, G. Yang, S. Miao, X. Liu, X. Bao, *J. Phys. Chem. A* **2004**, *108*, 6730–6734.

[12] C. Liu, I. Tranca, R. A. van Santen, E. J. M. Hensen, E. A. Pidko, *J. Phys. Chem. C* **2017**, *121*, 23520–23530.

[13] (a) M. S. Stavet, J. B. Nicholas, *J. Phys. Chem.* **1995**, *99*, 15046-15061. (b) S. P. Yuan, J. G. Wang, Y. W. Li, H. Jiao, *J. Phys. Chem. A* **2002**, *106*, 8167–8172.

[14] (a) M. F. Zalazar, D. J. R. Duarte, N. M. Peruchena, Adsorption of Alkenes on Acidic Zeolites. Theoretical Study Based on the Electron Charge Density, *J. Phys. Chem. A* **2009**, *113*, 13797–13807. (b) A. N. Petelski, N. M. Peruchena, S. C. Pamies, G. L. Sosa, *J. Mol. Model.* **2017**, *23*, 263.

[15] W. E. Farneth, R. J. Gorte, *Chem. Rev.* **1995**, *95*, 615–635.

[16] A. Bhan, W. N. Delgass, *Cat. Rev.: Sci. Eng.*, **2008**, *50*, 19–151.

[17] A. J. Jones, E. Iglesia, *ACS Catal.* **2015**, *5*, 5741−5755.

[18] M. Boronat, A. Corma, *ACS Catal.* **2019**, *9*, 1539−1548.

[19] Gaussian 16, Revision C.01, M. J. Frisch, G. W. Trucks, H. B. Schlegel, G. E. Scuseria, M. A. Robb, J. R. Cheeseman, G. Scalmani, V. Barone, G. A. Petersson, H. Nakatsuji, X. Li, M. Caricato, A. V. Marenich, J. Bloino, B. G. Janesko, R. Gomperts, B. Mennucci, H. P. Hratchian, J. V. Ortiz, A. F. Izmaylov, J. L. Sonnenberg, D. Williams-Young, F. Ding, F. Lipparini, F. Egidi, J. Goings, B. Peng, A. Petrone, T. Henderson, D. Ranasinghe, V. G. Zakrzewski, J. Gao, N. Rega, G. Zheng, W. Liang, M. Hada, M. Ehara, K. Toyota, R. Fukuda, J. Hasegawa, M. Ishida, T. Nakajima, Y. Honda, O. Kitao, H. Nakai, T. Vreven, K. Throssell, J. A. Montgomery, Jr., J. E. Peralta, F. Ogliaro, M. J. Bearpark, J. J. Heyd, E. N. Brothers, K. N. Kudin, V. N. Staroverov, T. A. Keith, R. Kobayashi, J. Normand, K. Raghavachari, A. P. Rendell, J. C. Burant, S. S. Iyengar, J. Tomasi, M. Cossi, J. M. Millam, M. Klene, C. Adamo, R. Cammi, J. W. Ochterski, R. L. Martin, K. Morokuma, O. Farkas, J. B. Foresman, D. J. Fox, Gaussian, Inc., Wallingford CT, 2016.

[20] Y. Zhao, D. G. Truhlar, *Theor. Chem. Acc.* **2008**, *120*, 215–241.

[21] G. J. Gomes, M. F. Zalazar, C. A. Lindino, F. R. Scremin, P. R. Bittencourt, M. Budke Costa, N. M. Peruchena, *Microporous Mesoporous Mater.* **2017**, *252*, 17–28. (b) G. J. Gomes, M. F. Zalazar, P. A. Arroyo, F. R. Scremin, M. Budke Costa, P. R. S. Bittencourt, C. A. Lindino, N. M. Peruchena, *ChemistrySelect*, **2019**, *4*, 3031-3041.

[22] Ch. Baerlocher, L. B. McCusker, Database of Zeolite Structures: http://www.iza-structure.org/databases/

[23] (a) G. J. Gomes, M. Budke Costa, P. R.S. Bittencourt, M. F. Zalazar, P. A. Arroyo, *Renewable Energy* **2021**, *178*, 1–12. (b) G. J. Gomes, M. F. Zalazar, P. A. Arroyo, *Top. Catal.* **2022**, *65*, 871–886. (c) G. J. Gomes, D. M. Dal Pozzo, M. F. Zalazar, M. B. Costa, P. A. Arroyo, P. R. S. Bittencourt, *Top. Catal.* **2019**, *62*, 874–883.

[24] L. W. Chung, W. M. C. Sameera, R. Ramozzi, A. J. Page, M. Hatanaka, G. P. Petrova, T. V. Harris, X. Li, Z. Ke, F. Liu, H.-B. Li, L. Ding, K. Morokuma, *Chem. Rev.* **2015**, *115*, 5678–5796.

[25] T. Lu, F. Chen, *J. Comb. Chem.* **2012**, *33*, 580–592.

[26] W. Humphrey, A. Dalke, K. Schulten, *J. Mol. Graphics* **1996**, *14*, 33–38.

[27] C. Fonseca Guerra, J.-W. Handgraaf, E. J. Baerends, F. M. Bickelhaupt, *J. Comput. Chem.* **2004**, *25*, 189–210.

[28] CYLview, 1.0b; C. Y., Legault, Université de Sherbrooke, **2009** (http://www.Cylview.Org).

[29] D. Rodrigues Silva, L. de Azevedo Santos, M. P. Freitas, C. Fonseca Guerra, T. A. Hamlin, *Chem. Asian. J.* **2020**, *15*, 4043–4054.

[30] I. Fernández, F. M. Bickelhaupt, D. Svatunek, *J. Chem. Theory Comput.* **2023**, *19*, 7300–7306.

[31] S. Sowlati-Hashjin, V. Ĉadek, S. Sadjadi, M. Karttunen, A. Martín-Pendás, C. Foroutan-Nejad, *Nat. Commun.* **2022**, *13*, 2069.

[32] C. Nieuwland, C. Fonseca Guerra, *Chem. Eur. J.* **2022**, *28*, e202200755.

[33] N. V. Vlasenko, Y. N. Kochkin, G. M. Telbiz, O. V. Shvets, P. E. Strizhak, *RSC Adv.* **2019**, *9*, 35957-35968.

[34] A. Auroux, *Top. Catal.* **2002**, *19*, 205–213.

[35] C. Lee, D. J. Parrillo, R. J. Gorte, W. E. Farneth, *J. Am. Chem. Soc.* **1996**, *118*, 13, 3262–3268.

[36] E. R. Johnson, S. Keinan, P. Mori-Sánchez, J. Contreras-García, A. J. Cohen, W. Yang, *J. Am. Chem. Soc.* **2010** *132*, 6498–6506.

[37] A. N. Petelski, S. C. Pamies, M. J. V. Márquez, G. L. Sosa, N. M. Peruchena, *ChemPhysChem* **2022**, *23*, e202200151.

[38] L. de Azevedo Santos, T. C. Ramalho, T. A. Hamlin, F. M. Bickelhaupt, *Chem. Eur. J.* **2023**, *29*, e202203791.

[39] (a) M. F. Zalazar, N. D. Cabral, G. D. Romero Ojeda, C. I. A. Alegre, N. M. Peruchena, *J. Phys. Chem. C.* **2018**, *122*, 27350–27359. (b) M. F. Zalazar, E. N. Paredes, G. D. Romero Ojeda, N. D. Cabral, N. M. Peruchena, *J. Phys. Chem. C.* **2018**, *122*, 3350–3362.

[40] P. Sahu, A. Sakthivel, *Mater. Sci. Energy Technol.* **2021**, *4*, 307–316.

[41] R. E. Patet, M. Koehle, R. F. Lobo, S. Caratzoulas, D. G. Vlachos, *J. Phys. Chem. C* **2017**, *121*, 13666−13679.

Table of Contents

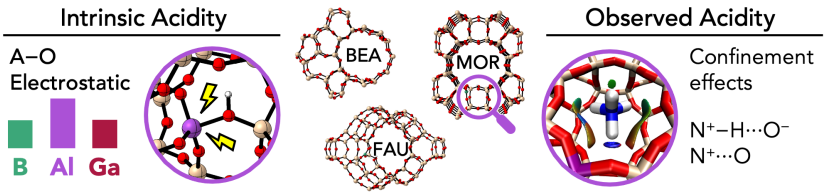

Electrostatic control: the stronger acidity of aluminum substituted zeolites comes from a stronger Al–O bond governed by electrostatic interaction. The acidity measured with ammonia is influenced by the topology of the zeolite and the charge distribution exerted by the substituent element within the cavity. These factors determine the confinement interactions, and thus the average acidity.

Institute and/or researcher Twitter usernames: @NicolaiAndre, @facenaunne, @CONICETNordeste, @CONICETDialoga, @Quitex_UTN, @UTN_FRRE

WILEY-VCH